ELSEVIER

Chemical Engineering Journal 139 (2008) 296–303

Chemical Engineering Journal

www.elsevier.com/locate/cej

Flux enhancement and cake formation in air-sparged cross-flow microfiltration

Kuo-Jen Hwang *, Ya-Ju Wu

Department of Chemical and Materials Engineering, Tamkang University, Tamsui, Taipei Hsien 25137, Taiwan

Received 24 October 2006; received in revised form 28 July 2007; accepted 3 August 2007

Abstract

The flux enhancement in cross-flow microfiltration of submicron particles by sparged air-bubble is studied. The effects of operating conditions, such as air-bubble velocity, suspension velocity and filtration pressure, on the cake properties and filtration flux are discussed thoroughly. The results show that the pseudo-steady filtration flux increases as the air-bubble velocity and filtration pressure increase. The sparged air-bubble can significantly improve filtration flux, but the flux enhancement is more remarkable in the lower air-bubble velocity region. A gas–liquid two-phase flow model is adopted for estimating the shear stress acting on the membrane surface under various operating conditions. The cake mass can be significantly reduced by increasing the shear stress acting on the membrane surface. However, the SEM analysis illustrates that the particle packing structure becomes more compact as the air-bubble velocity increases. This results in a slightly higher average specific cake filtration resistance under higher air-bubble velocity. Consequently, a minimum flux occurs at the critical shear stress, e.g., $\tau_w = 1.1\ N/m^2$ in this study, when these effects are both taken into consideration. As the shear stress increases by increasing the suspension or gas-bubble velocity, the filtration flux decreases in the low shear stress region but, on the contrary, quickly increases in the high shear stress region. Furthermore, a force balance model is derived for understanding the particle deposition on the membrane surface. The relationship among filtration flux, shear stress and overall filtration resistance is obtained and verified by experimental data.

Keywords: Cross-flow microfiltration; Flux enhancement; Air-bubble sparging; Particle deposition; Cake properties

1. Introduction

Cross-flow microfiltration is an efficient and energy-saving method for separating fine particles from liquids in many chemical, environmental, biochemical and materials processes. Although this filtration mode has many advantages, the flux decline due to the membrane fouling becomes a severe barrier for its further developments and wide applications. In order to enhance the filtration flux and reduce the membrane fouling, many efforts have been paid previously, e.g., placing protuberances onto the membrane surface, placing objects into the flow channel, generating a pulsating flow, producing the Taylor or Dean vortices, etc. [1]. The main concept or purpose of these methods is to produce turbulent perturbations which can restrain suspension particles to deposit on the membrane surface. Based on this concept, increasing the shear stress acting on the membrane surface by sparging air-bubbles into the filter channel may reduce the particle deposition and enhance filtration flux. This method is indeed worth for further development due to its low operating cost and easy operation; however, the complex hydrodynamic phenomena influencing the operating performance should be carefully analyzed.

The effect of sparged air-bubble on the microfiltration efficiency has been investigated by a few previous studies. Mercier-Bonin et al. [2,3] carried out the cross-flow microfiltration of baker yeast and enzyme/yeast mixtures. They claimed that the sparged air-bubble could efficiently enhance the filtration flux and enzyme recovery. Al-akoum et al. [4] used cross-flow filtration for separating yeast cells from an aqueous suspension. They tried to employ three hydrodynamic methods in their experiments to enhance filtration flux, such as a vibration membrane, injecting gas-bubble, and generating Dean Vortices. They concluded that all filtration fluxes were increased by increasing the shear stress acting on the membrane surface using these methods. Derradji et al. [5] and Xu et al. [6] installed a turbulence promoter before the filter membrane. They found

* Corresponding author. Fax: +886 2 26209887.
E-mail address: kjhwang@mail.tku.edu.tw (K.-J. Hwang).

1385-8947/$ – see front matter © 2007 Elsevier B.V. All rights reserved.
doi:10.1016/j.cej.2007.08.006

Nomenclature

A	cross-sectional area of the filter channel, (m^2)
C_1	correction factor defined in Eq. (11)
C_2	correction factor defined in Eq. (12)
C_3–C_6	coefficients defined in Eqs. (15)–(17)
d_p	diameter of particles, (m)
F_i	net interparticle force, (N)
F_n	drag force exerted on particles in the filtration direction, (N)
F_t	drag force exerted on particles in the suspension flow direction, (N)
f_c	friction coefficient between particles
H	the clearance of the filter channel, (m)
L_f	the length of the filter channel, (m)
n	the empirical exponent in Eqs. (3) and (4)
P	hydraulic pressure, (N/m^2)
ΔP	filtration pressure, (N/m^2)
Q	volumetric flow rate, (m^3/s)
q	superficial velocity of filtrate or filtration flux, (m^3/m^2 s)
q_s	pseudo-steady state filtration flux, (m^3/m^2 s)
R_c	resistance of the filter cake, (m^{-1})
R_m	resistance of the filter membrane, (m^{-1})
R_t	overall filtration resistance, (m^{-1})
u	superficial velocity, (m/s)
v	true velocity, (m/s)
W	the width of the filter channel, (m)
w_c	mass of dry cake per unit area, (kg/m^2)
X	the parameter defined in Eq. (2)
x	distance from the inlet of filter channel in suspension flow direction, (m)

Greek Letters

α_{av}	average specific filtration resistance of cake, (m/kg)
ϕ_g	the multiplier defined in Eq. (1)
ϕ_l	the multiplier defined in Eq. (1)
λ	void fraction in gas–liquid two-phase flow
μ	viscosity of liquid, (kg/s m)
θ	gas injection factor defined in Eq. (18)
ρ	density, (kg/m^3)
τ_w	shear stress acting on the membrane surface, (N/m^2)

Subscripts

g	gas
l	liquid
go	gas-only
lo	liquid only
tp	two phase

that the fluxes were increased 180% and 2.5-fold, respectively, under air-bubble sparging. Mikulášek et al. [7] and Pospišil et al. [8] also found the existence of air-bubble flow could increase the filtration flux. They derived a correlation between flux and hydrodynamic conditions based on the material balance and the filtration equation. However, the used parameters, e.g., gas-flow factor, should be determined in experiments.

Chang and Fane [9,10], Chang et al. [11], and Fane et al. [12] used organic hollow fibers with different arrangements to perform cross-flow filtration of yeast cells. They tried to introduce the air-bubbles flowing among hollow fibers in order to restrain membrane fouling and enhance filtration flux. The effects of the orientation and clearance of fibers, the fiber diameter, and the ratio of liquid to gas flow rate on the filtration flux were discussed. A dimensionless group based on hydrodynamics was set as the parameter to simulate the flux distribution in the axial direction of hollow fibers [10,12]. They also found in experiments that the fouling could be reduced more efficiently by the air-bubbles if the fiber axis was parallel to the fluid flow direction. In conclusion, increasing the shear stress and generating vortices were efficient ways to enhance filtration flux.

As mentioned above, most previous studies used experimental analysis methods to understand the flux enhancement by sparged air-bubbles. Although the operating variables can be correlated into some empirical equations, most parameters should be determined by performing a series of experiments, and the results are hard to relate to actual hydrodynamic conditions. In this study, hydrodynamic models for calculating the shear stress acting on the membrane surface and the critical condition for particle deposition are derived. Effects of operating conditions, such as the velocities of air-bubble and suspension flows and the filtration pressure, on the filtration flux and cake properties are discussed.

2. Theory

2.1. Shear stress acting on the membrane surface

Fig. 1 shows a schematic diagram of a multi-phase cross-flow microfiltration in a two-parallel-plate microfilter with a porous bottom plate. The suspension flows across the membrane surface tangentially, while the filtrate permeates vertically. Fine particles are carried by the liquid to migrate in the filter channel, and some of them have opportunities to arrive at the membrane surface and deposit stably to form a filter cake. Since the cake growth is limited by the shear stress produced by the tangential multi-phase flow, to estimate the shear stress is the main gate for understanding the filtration performance. In this study, the

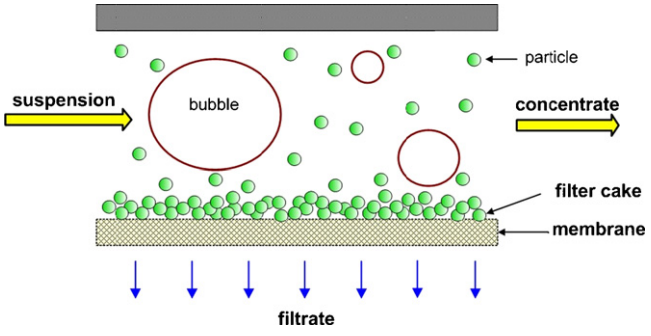

Fig. 1. Schematic diagram of multi-phase cross-flow microfiltration.

model derived by Wilkes [13] is adopted to evaluate the pressure gradient in the filter channel. According to this model, the pressure gradient of a liquid–gas two-phase flow, $(dP/dx)_{tp}$, can be calculated by

$$\left(\frac{dP}{dx}\right)_{tp} = \phi_g^2\left(\frac{dP}{dx}\right)_{go} = \phi_l^2\left(\frac{dP}{dx}\right)_{lo} \quad (1)$$

where ϕ_g and ϕ_l are the multipliers used for obtaining two-phase pressure gradient, while $(dP/dx)_{go}$ and $(dP/dx)_{to}$ are the pressure gradients of gas- and liquid-only flowing by itself and occupying the entire cross-section of the conduit, respectively. The value of $(dP/dx)_{go}$ or $(dP/dx)_{to}$ can be obtained by solving the well-known "Hagen–Poiseuille law".

The square of the parameter X is defined as the ratio of ϕ_g^2 to ϕ_l^2, that is,

$$X^2 = \frac{(dP/dx)_{lo}}{(dP/dx)_{go}} = \frac{\phi_g^2}{\phi_l^2} \quad (2)$$

The relations between X and ϕ values under various void fractions have been measured in previous experiments [14]. Based on the simplified model [13], the friction factor is assumed as the same for both gas- and liquid-phase. Hence, the value of X^2 can be calculated from the density and superficial velocity of both phases, that is,

$$X^2 = \frac{(dP/dx)_{lo}}{(dP/dx)_{go}} = \frac{\rho_l u_l^2}{\rho_g u_g^2} \quad (3)$$

Moreover, a general form for correlating ϕ_g and ϕ_l can be expressed as [13]:

$$\frac{1}{(\phi_g^2)^{1/n}} + \frac{1}{(\phi_l^2)^{1/n}} = 1 \quad (4)$$

Substituting Eq. (4) into Eq. (2) and eliminating ϕ_g gives

$$\phi_l = \left(\frac{1 + X^{2/n}}{X^{2/n}}\right)^{n/2} \quad (5)$$

The exponent, n, under various flow conditions were measured and tabulated in Wilkes [13]. Since the data were obtained in a wide variety of liquids flowing with air in small-diameter tubes, the deviation due to the assumption of the same friction factor for both phases in the simplified model may be modified and reduced. Therefore, the pressure gradient for gas–liquid two-phase flow can be estimated by Eq. (1) when ϕ_l is calculated by solving Eq. (5).

If the width, W, and the length, L_f, of the microfilter shown in Fig. 1 are much larger than the clearance, H, and the tangential flow rate is greatly higher than the filtrate flow rate, a momentum balance on the filter channel can be expressed as:

$$P(WH) - \left(P + \frac{dP}{dx}L_f\right)(WH) - \tau_w(2L_fW) = 0 \quad (6)$$

or

$$\tau_w = \frac{H}{2}\left(-\frac{dP}{dx}\right) \quad (7)$$

Thus, the shear stress acting on the membrane surface, τ_w, can be calculated by Eq. (7) once the pressure gradient is obtained by Eq. (1).

On the other hand, the void fraction, λ, in a gas–liquid two-phase flow can be empirically correlated by [13]

$$\lambda = \frac{1}{(1 + 0.0904X^{0.548})^{2.82}} \quad (8)$$

Therefore, the true velocities of gas and liquid flows can be calculated, respectively, by:

$$v_g = \frac{Q_g}{\lambda A}, \qquad v_l = \frac{Q_l}{(1-\lambda)A} \quad (9)$$

in which A is the cross-sectional area of the channel, while Q_g and Q_l are the volumetric flow rates of gas and liquid, respectively. In general, the suspension velocity in the filter chamber will be enhanced by an air-bubble sparging.

2.2. Force balance model for particle deposition

In previous studies, many models were proposed for explaining the particle transportation and deposition in cross-flow microfiltration, e.g., the concentration polarization models, hydrodynamic models, and membrane blocking models [1]. The particle size or the ratio of the particle size to the membrane pores is always the key parameter for choosing an applicable one in those models. Concentration polarization occurs when the particle diffusion flux is dominant, while the membrane blocking model can be employed when the particle size is smaller than or comparable to the membrane pores. In this study, differing from those "particle depolarization mechanisms" such as diffusion and inertial lift, the particles are carried to the membrane surface by the filtrate flow, and the stability of the depositing particles is determined by the forces exerted on them.

If the net gravitational force and the inertial lift force exerted on the depositing particles are much smaller than the drag forces and interparticle forces, the force balance model at the pseudo-steady condition can be simplified as [15,16]:

$$F_t = f_c(F_n + F_i) \quad (10)$$

where f_c is the friction coefficient between particles, while F_i is the net interparticle force (including the electrostatic force, Van der Waals force, etc.), and F_t and F_n are the drag forces in the tangential and filtration directions, respectively. According to Eq. (10), if the tangential force exerted on a particle staying on the membrane or cake surface exceeds the friction force, the particle will be swept away from its original location and be transported back to the bulk suspension flow. Otherwise, the particle can deposit stably.

Based on the analysis of Hwang and Lin [16], the tangential drag force can be estimated by the modified Stokes law since the low Reynolds number near the membrane surface, that is,

$$F_t = C_1 d_p^2 \tau_w \quad (11)$$

where d_p is the particle diameter and C_1 is a correction factor for the existences of the filter cake and the membrane. If the par-

ticle size distribution is uniform, the tangential force is directly proportional to the shear stress acting on the membrane surface.

The normal drag can also be calculated by using the modified Stokes law since the Reynolds number in the filtration direction is also very low in most conditions, that is,

$$F_n = 3\pi\,\mu\,d_p\,q_s\,C_2 \tag{12}$$

where μ is the fluid viscosity, while q_s the pseudo-steady flux. The correction factor, C_2, can be obtained by applying the results of Goren [17]:

$$C_2 = \left(\frac{R_t d_p}{3} + 1.07^2\right)^{1/2} \tag{13}$$

where R_t is the overall filtration resistance which can be obtained by summing the filtration resistances of cake and membrane, i.e.,

$$R_t = R_c + R_m = w_c\,\alpha_{av} + R_m \tag{14}$$

in which w_c and α_{av} are the mass and average specific filtration resistance of cake, respectively. Since the value of $R_t \times d_p$ is much larger than 1.07^2 in most conditions, Eq. (12) can be rewritten as below for simplicity:

$$F_n = C_3\,\mu\,d_p^{1.5}\,q_s\,R_t^{0.5} \tag{15}$$

However, the coefficient C_3 should be taken the existence of air-bubbles into account. Because the bubble pattern is strongly dependent on the local hydraulic pressure [13], this coefficient can be considered to be a function of filtration pressure.

The interparticle forces for submicron particles can be estimated by the well-known "DLVO theory". Two major long-range interparticle forces, Van der Waals force and electrostatic force, can be obtained based on a pair-wise assumption. However, the net interparticle force is assumed to be constant under a fixed particle surface potential and electrolyte concentration in our model for simplicity.

Substituting Eqs. (11) and (15) into Eq. (10), the force balance equation for a uniform particle size distribution can be expressed as:

$$\tau_w = C_4\,\mu\,q_s\,R_t^{0.5} + C_5 \tag{16}$$

or be rearranged as:

$$q_s = C_6\frac{\tau_w - C_5}{\mu\,R_t^{0.5}} \tag{17}$$

Therefore, the relationship among the pseudo-steady filtration flux, shear stress and overall filtration resistance under a given filtration pressure can be given by Eq. (16).

3. Materials and methods

A kind of spherical particles made of Polymethly methacrylate (PMMA) was used as the submicron particulate sample in experiments. The particles had a very narrow size distribution with a mean diameter of 0.4 μm. The density of the particles was 1219 kg/m^3. The particles were suspended in de-ionized water to prepare a 0.1 wt% suspension. The pH value and temperature were kept at 7.0 and 20 °C, respectively, during filtration. The zeta potential of particles in such a condition was −25 mV. The membrane made of cellulose ester with a mean pore size of 0.22 μm was used in experiments as the filter medium.

A schematic diagram of the cross-flow microfiltration system used in this study is shown in Fig. 2. The two-parallel-plate microfilter had a clearance of 1.0×10^{-3} m, a width of 2.0×10^{-2} m, and a length of 5.0×10^{-2} m. Before an experiment, the particles were suspended uniformly in the suspension tank by a magnetic mixer. The flow rates of the suspension and the sparged-air were adjusted and measured by the rotameters (A) and (B), respectively. The filtration pressure was adjusted carefully to a set value by the needle valve. Any increase in the filtrate weight during filtration could be detected by the load cell and recorded via a personal computer. An appropriate amount of make-up water was duly added into the suspension tank to keep a constant suspension concentration during the filtration. The size and frequency of the air-bubbles in the filter channel could be detected and recorded by a video recorder. When the

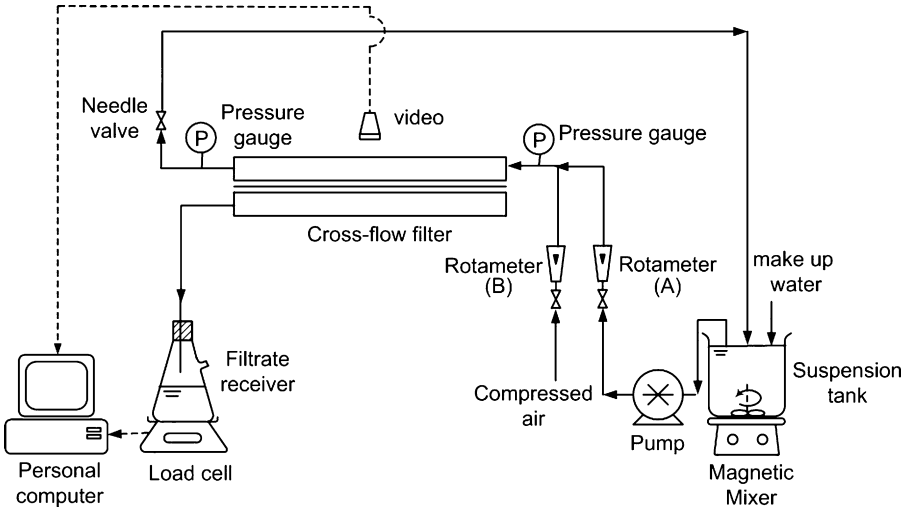

Fig. 2. A schematic diagram of cross-flow microfiltration system.

experiment was terminated, the cake formed on the filter membrane was sent to analyze its wet and dry mass by an ORION moisture titrator or observe the particle packing structure using SEM analysis.

4. Results and discussion

Liquid–gas two-phase flow in a conduit can be divided into three typical patterns according to the injection factor [18]. The injection factor is defined as [18]:

$$\theta \equiv \frac{u_g}{u_g + u_l} \tag{18}$$

Based on the analysis of Cabassud et al. [18], the flow pattern is bubble flow when $\theta < 0.2$, is slug flow when $0.2 < \theta < 0.9$, and is annular flow as $\theta > 0.9$. Comparing the operating conditions in this study, the suspension flow can be considered to be a slug flow. Because a slug flow may produce a higher wall shear rate and higher turbulence, the flux enhancement by the sparged air-bubbles can be expected.

Fig. 3 shows the time courses of filtration flux in cross-flow microfiltration under various air-bubble sparged intensities (air-bubble velocities). The Reynolds numbers of suspension and air-bubble flows are both smaller than 1000 within the operating conditions of this study; consequently, the flow pattern in both phases can be considered to be laminar. The values of void fraction, λ, under various conditions are calculated by solving Eq. (8) and listed in Table 1. The values of λ are set to be smaller than 0.3 in this study. At the beginning of filtration, the filtration fluxes under different air-bubble velocities are almost all the same since no any cake has been formed yet. The filtration resistance is only attributed to the filter membrane at that time. The curve trend shown in Fig. 3 is similar to those in previous studies [15,16]. The filtration flux attenuates very quickly when a filter cake begins to be formed on the membrane surface and then gradually approaches a pseudo-steady value after 4000 s. The curves shown in the figure clearly indicate that the flux decay would be restrained by the sparged air-bubbles. The more intense the sparged air-bubble is, the higher the filtration flux will be obtained. This result reveals the filtration flux can be efficiently enhanced by a sparged air-bubble.

Table 1
The values of void fraction under various conditions.

u_l (m/s)	u_g (m/s)	λ
0.1	0.02	0.076
	0.04	0.137
	0.08	0.224
	0.12	0.285
0.2	0.04	0.080
0.3		0.055
0.4		0.041
0.5		0.032

The values of pseudo-steady filtration flux under various air-bubble velocities and filtration pressures are co-plotted in Fig. 4. As shown in Fig. 3, more sparged air-bubbles may result in a higher filtration flux due to the greater shear stress acting on the membrane surface. However, the degree of flux enhancement at the pseudo-steady-state becomes moderate and slow down as air-bubble velocity increases. The flux can be increased 75% when the superficial air-bubble velocity increases from 0 to 0.12 m/s. Moreover, the effect of filtration pressure on the pseudo-steady flux is also shown in Fig. 4. An increase in filtration pressure leads to a higher filtration flux due to the higher filtration driving force. A 50% flux increase can be obtained as the filtration pressure increases from 20 to 100 kPa. It can be noticed that the flux does not linearly increase with filtration pressure since the fluxes are all higher than the critical flux. This implies that the cake properties, such as the mass and specific filtration resistance of cake, play important roles in determining the filtration flux.

Fig. 5 shows the cake mass formed on the membrane surface under various gas-bubble velocities and filtration pressures. A sparged-air can significantly reduce the cake formation on the membrane surface, i.e., the cake mass decreases with the increase of air-bubble velocity. This indicates that sparging air-

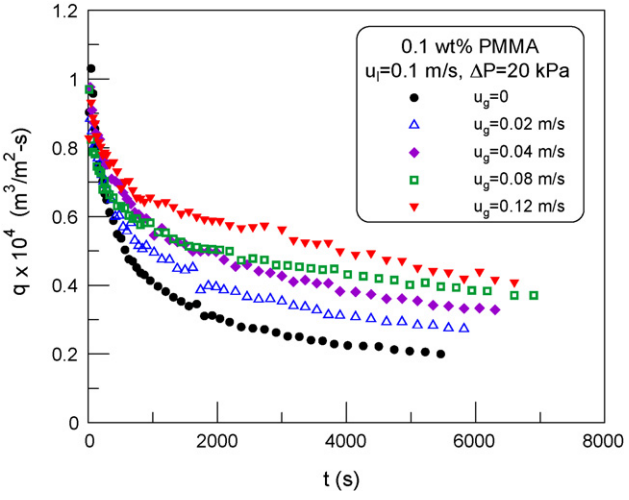

Fig. 3. The time courses of filtration flux during cross-flow microfiltration with different velocities of air-bubble injection.

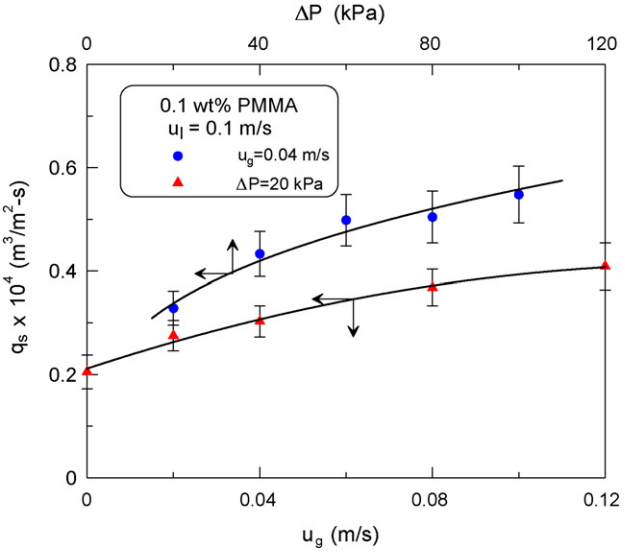

Fig. 4. The pseudo-steady filtration fluxes under various air-bubble velocities and filtration pressures.

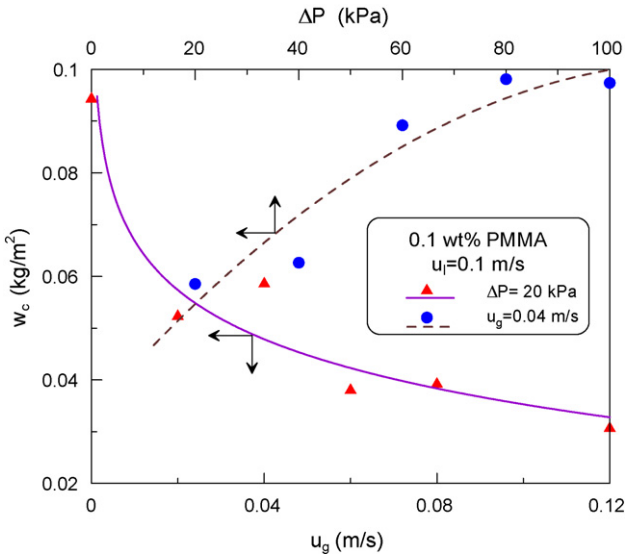

Fig. 5. Effects of air-bubble velocity and filtration pressure on the cake mass.

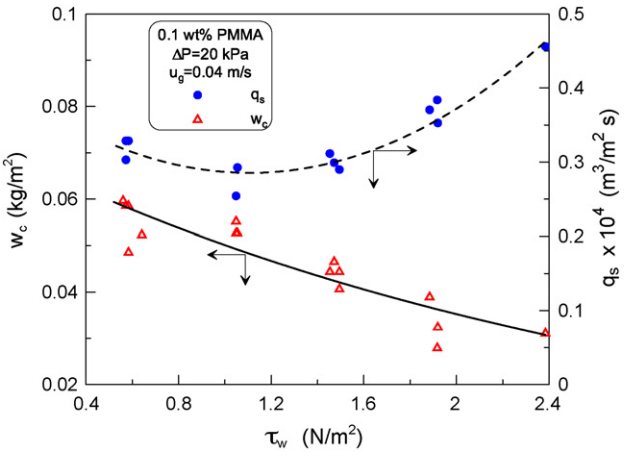

Fig. 7. Effect of wall shear stress on the cake mass and the pseudo-steady filtration flux.

bubbles is an efficient way in reducing cake formation. The cake mass under $u_g = 0.12$ m/s is only 30% of that in the condition of no sparged air-bubble. This phenomenon can reasonably explain why the filtration flux can be enhanced by sparged air-bubble. On the other hand, the cake mass also increases with increasing filtration pressure. This is because the particles staying on the membrane are more stable, or in other words, are more easily to deposit, under a higher filtration flux [15]. Although the filtration resistance may be increased due to the increase of cake mass, the higher pressure is still enough to drive a higher filtration flux (refer to Fig. 4).

In order to understand how the true velocity and wall shear stress in the filter channel are affected by the sparged air-bubbles, the gas–liquid two-phase flow model described previously are adopted to calculate the true velocities of suspension and air-bubble flows as well as the shear stress acting on the membrane surface. Fig. 6 shows the effect of superficial suspension velocity on these variables under a fixed air-bubble superficial velocity. Indeed, the true velocities and the wall shear stress are increased linearly with the increase of superficial suspension velocity. When the superficial suspension velocity increases from 0.1 to 0.5 m/s under the condition of $u_g = 0.04$, the true suspension

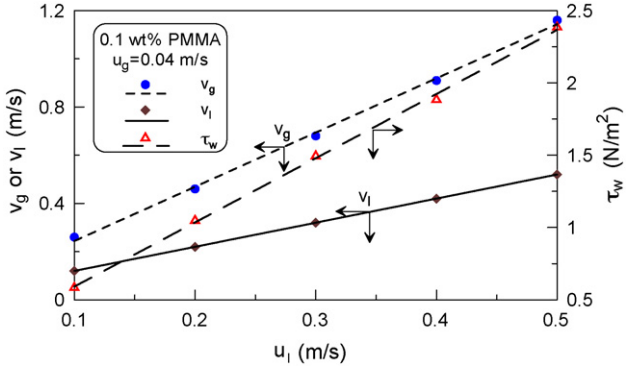

Fig. 6. The true velocities of gas-bubble and suspension flow and the wall shear stresses under values suspension flow rates.

velocity is increased 5–20% due to the air-bubble sparging, while the true air velocity increases 6–30-fold. As a result, the wall shear stress increases 4-fold as u_l increases from 0.1 to 0.5 m/s. This increase of wall shear stress causes the particle deposition on the membrane surface to be harder, and, of course, to a higher filtration flux.

According to above analysis, increasing the wall shear stress by sparging air-bubbles in order to reduce the cake growth seems to be an effective way for enhancing the filtration flux in cross-flow filtration. The effects of wall shear stress on the cake mass and filtration flux are shown in Fig. 7. The shear stress shown in this figure is calculated by the two-phase flow model described previously. From the regressed curve of those scattered data, it can be seen that the cake mass decreases markedly with the increase of the wall shear stress. This phenomenon reveals that increasing the wall shear stress is an efficient method to reduce the cake formation. However, as shown in Fig. 7, the filtration flux slightly decreases as τ_w increases from 0.6 to 1.1 N/m^2. When τ_w exceeds 1.1 N/m^2, the flux significantly increases with the increase of τ_w. Since the critical shear stress, 1.1 N/m^2, results in a minimum flux, the cake mass should not be the sole factor affecting the overall filtration flux. In order to understand why this concave flux trend occurs, the filtration resistances and cake properties under various operating conditions are analyzed below.

In most microfiltration, the cake resistance plays the major role in determining the overall filtration resistance. Based on the conventional filtration theory, the cake filtration resistance can be expressed as the product of the mass and average specific filtration resistance of cake, e.g., Eq. (14). Therefore, the average specific filtration resistance of cake is another important factor to affect the overall filtration resistance. Fig. 8 depicts the average specific filtration resistance of cake under various velocities of air-bubble and suspension flows. From the regressed curves shown in this figure, one can find the value of α_{av} increases with both increasing u_l and u_g. These imply that the cake structure becomes more compact under a higher u_l or u_g. Another interesting phenomenon is that a sudden increase in α_{av} can be found if the operation changes from none to an air-bubble sparging.

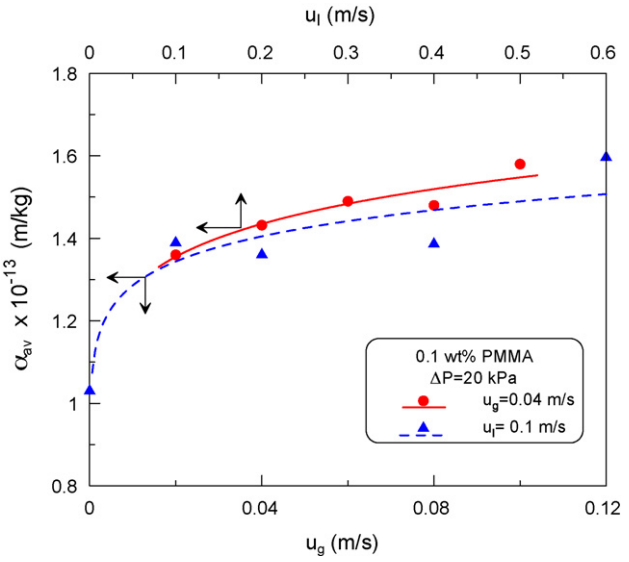

Fig. 8. Effects of air-bubble and suspension velocities on the average specific filtration resistance of cake.

This may be attributed to the different particle packing structures between the cases of whether air-bubble sparging or not. This inference has been demonstrated by a SEM analysis which is shown in Fig. 9. Fig. 9(a and b) are the SEM photographs taken under the conditions of $u_g = 0$ and $u_g = 0.12$, respectively. Comparing these two photos, it can be found that the particle packing becomes more regular and more compact under a condition of air-bubble sparging. This fact can reasonably explain the tendency of α_{av} as shown in Fig. 8.

According to the results shown in Figs. 7 and 8, the cake mass monotonically decreases but the specific filtration resistance of cake increases as the suspension velocity (or wall shear stress) increases. These two contrary factors may construct of a convex trend in the overall filtration resistance as u_l (or τ_w) increases. Since the variation in α_{av} is more remarkable under a low suspension velocity, the increase in filtration resistance leads the filtration flux to decrease when the suspension velocity increases from 0.1 to 0.2 m/s (or τ_w increases from 0.6 to 1.1 N/m^2). However, the variation in α_{av} in high suspension velocity region becomes trivial. An increase in suspension velocity or wall shear stress induces a decrease in cake mass, a decrease in the overall filtration resistance, and hence an increase in filtration fluxes. Thus, the effects of operating conditions on the filtration flux can be well understood when the cake mass and the particle packing structure are simultaneously taken into consideration.

According to the proposed force balance model for the particle deposition on the membrane surface, the relationship among the pseudo-steady filtration flux, the wall shear stress and the overall filtration resistance can be correlated by Eq. (16). This equation reveals a linear relation between $\mu q_s R_c^{0.5}$ and τ_w if the membrane resistance is negligible small compared to the cake resistance. Fig. 10 is a plot of $\mu q_s R_c^{0.5}$ versus τ_w under a fixed filtration pressure of 20 kPa. Although the experimental data are measured under various suspension and gas-bubble velocities, they can be regressed to a single straight line. This demonstrates the reliability and practicability of the force balance model, and

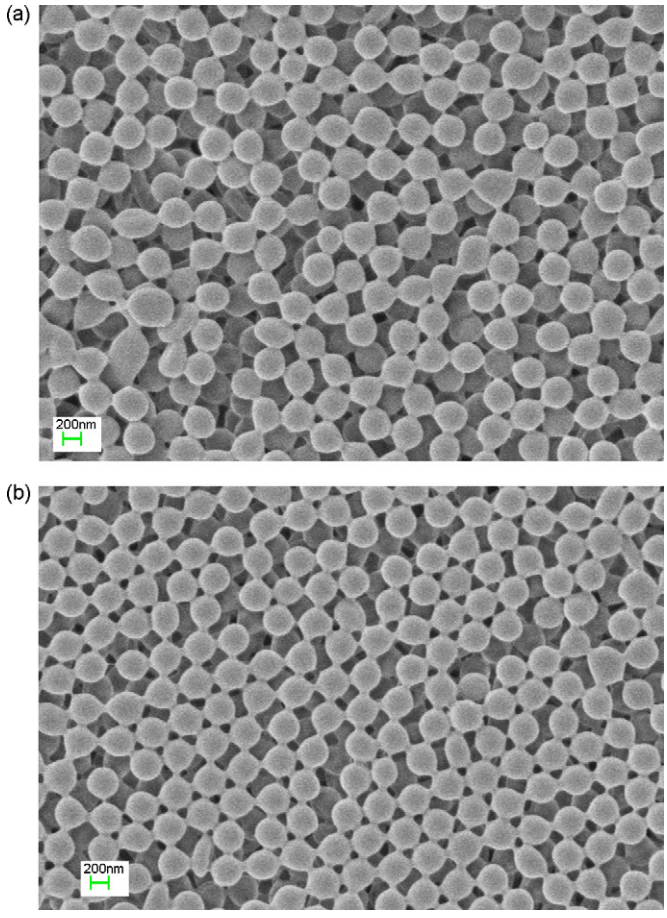

Fig. 9. Top view of particle packing structures under $u_l = 0.1$ m/s and $\Delta P = 20$ kPa (SEM × 50,000), (a) $u_g = 0$, (b) $u_g = 0.12$ m/s.

the coefficients in Eq. (16) can be obtained from the slope and intercept of the straight line. Since the shear stress on the membrane surface can be estimated by the gas–liquid two-phase flow model, the pseudo-steady filtration flux can then be predicted by solving Eq. (16) once the cake resistance is known. Unfortunately, as shown in Figs. 8 and 9, the existence of air-bubbles

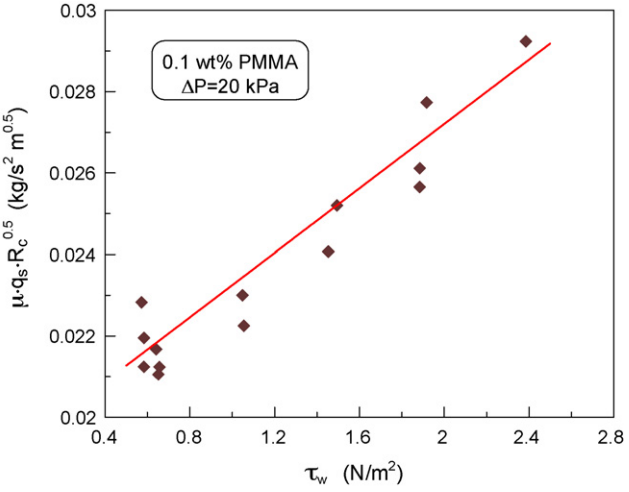

Fig. 10. A plot of $\mu q_s R_c^{0.5}$ vs. τ_w.

causes the filter cake to be a more compact packing structure and to a sudden increase in the average specific filtration resistance. But it is still lack of the quantitative prediction for the values of α_{av} under various conditions. This is worth to pay more attentions and efforts in the future, especially for the particle packing structures under different air-bubble sparging intensities. However, this study provides a method to quantitatively relate the filtration flux to operating conditions.

5. Conclusion

The effects of operating conditions, such as air-bubble velocity, suspension velocity and filtration pressure, on the cake properties and filtration flux in air-bubble sparged cross-flow microfiltration have been discussed. The pseudo-steady filtration flux increased with increasing air-bubble velocity and filtration pressure. The sparged air-bubbles could significantly enhance filtration flux, e.g., the flux increased 75% when the superficial air-bubble velocity increased from 0 to 0.12 m/s. However, the flux enhancement was more remarkable under lower air-bubble velocity region. A two-phase flow model was adopted for estimating the shear stress acting on the membrane surface. An increasing in shear stress could significantly reduce the cake mass but simultaneously increase the average specific filtration resistance of cake. A minimum filtration flux hence occurred under a critical shear stress of 1.1 N/m^2. The flux increased with increasing shear stress as τ_w exceeded that critical value. Furthermore, a linear relationship between $\mu q_s R_c^{0.5}$ and τ_w was derived by a force balance model and was demonstrated by experimental data.

Acknowledgement

The authors wish to express their sincere gratitude to the National Science Council of the Republic of China for its financial support.

References

[1] G. Belfort, R.H. Davis, A.L. Zydney, The behavior of suspensions and macromolecular solutions in crossflow microfiltration, J. Membr. Sci. 96 (1994) 1.

[2] M. Mercier-Bonin, C. Lagane, C. Fonade, Influence of a gas/liquid two-phase flow on the ultrafiltration and microfiltration performances: case of a ceramic flat sheet membrane, J. Membr. Sci. 180 (2000) 93.

[3] M. Mercier-Bonin, C. Fonade, Air-sparged microfiltration of enzyme/yeast mixtures: determination of optimal conditions for enzyme recovery, Desalination 148 (2002) 171.

[4] O. Al-akoum, M. Mercier-Boninb, L. Ding, C. Fonade, P. Aptel, M. Jaffrin, Comparison of three different systems used for flux enhancement: application to crossflow filtration of yeast suspensions, Desalination 147 (2002) 3l.

[5] A.F. Derradji, A. Bernabeu-Madico, S. Taha, G. Dorange, The effect of a static mixer on the ultrafiltration of a two-phase flow, Desalination 128 (2000) 223.

[6] N. Xu, W. Xing, N. Xu, J. Shi, Study on ceramic membrane bioreactor with turbulence promoter, Sep. Purif. Technol. 32 (2003) 403.

[7] P. Mikulášek, P. Pospišil, P. Dolecek, J. Cakl, Gas–liquid two-phase flow in microfiltration mineral tubular membranes: relationship between flux enhancement and hydrodynamic parameters, Desalination 146 (2002) 103.

[8] P. Pospišil, R.J. Wakeman, I.O.A. Hodgson, P. Mikulášek, Shear stress-based modelling of steady-state permeate flux in microfiltration enhanced by two-phase flows, Chem. Eng. J. 97 (2004) 257.

[9] S. Chang, A.G. Fane, Filtration of biomass with axial inter-fibre upward slug flow: performance and mechanisms, J. Membr. Sci. 180 (2000) 57.

[10] S. Chang, A.G. Fane, The effect of fibre diameter on filtration and flux distribution—relevance to submerged hollow fibre modules, J. Membr. Sci. 184 (2001) 221.

[11] S. Chang, A.G. Fane, S. Vigneswaran, Experimental assessment of filtration of biomass with transverse and axial fibres, Chem. Eng. J. 87 (2002) 121.

[12] A.G. Fane, S. Chang, E. Chardon, Submerged hollow fibre membrane module-design options and operational considerations, Desalination 146 (2002) 231.

[13] J.O. Wilkes, Fluid Mechanics for Chemical Engineers, Prentice Hall, New Jersey, USA, 2006, Chap.10, pp.468–474.

[14] R.W. Lockhart, R.C. Martinelli, Proposed correlation of data for isothermal two-phase, two-component flow in pipes, Chem. Eng. Progr. 45 (1) (1949) 39.

[15] W.M. Lu, K.J. Hwang, Cake formation in 2-D cross-flow filtration, AIChE J. 41 (6) (1995) 1443.

[16] K.J. Hwang, K.P. Lin, Cross-flow microfiltration of dual-sized submicron particles, Sep. Sci. Technol. 37 (2002) 2231.

[17] S.L. Goren, The hydrodynamic force resisting the approach of a sphere to a plane permeable wall, J. Colloid Interf. Sci. 69 (1979) 78.

[18] C. Cabassud, S. Laborie, L. Durand-Bourlier, J.M. Lainé, Air sparging in ultrafiltration hollow fibers: relationship between flux enhancement, cake characteristics and hydrodynamic parameters, J. Membr. Sci. 181 (2001) 57.